Biomechanics of the Optic Nerve Head*

J C Downs, M D Roberts, and C F Burgoyne, Devers Eye Institute, Portland, OR, USA

Glossary

Anisotropic materials – These materials exhibit higher or lower stiffness properties along different directions. For instance, concrete may be isotropic by itself, but the introduction of rebar during fabrication would produce an anisotropic material with higher resistance to tension along the direction of the rebar.

Elastic materials – These materials exhibit no time-dependent stress–strain behavior.

Isotropic materials – These materials exhibit identical resistance to load in all directions.

Linear materials – These materials exhibit a stress–strain relationship in which stress is directly proportional to strain by a constant factor known as the Young's modulus.

Material properties – These describe the ability of a tissue to resist deformation under applied load and therefore relate stress to strain (i.e., load to deformation). Material properties can be thought of as the stiffness or compliance of a particular tissue or material that is intrinsic to the material itself. These properties are often described in terms of their material symmetry (isotropic or anisotropic), the nature of the relationship between load and deformation (linear or nonlinear), and the time dependence of their response to loading (elastic or viscoelastic).

Mechanical failure – It occurs at even higher strain, typically follows yield, and generally manifests in soft tissues as catastrophic rupture or pulling apart.

Mechanical yield – It occurs when a material is strained beyond its elastic limit, and is therefore unable to return to its undeformed shape. A material or tissue that has yielded in response to high strains is permanently damaged and deformed and is usually less resistant to further loading (hypercompliance).

Nonlinear materials – These materials have a varying proportionality between stress and strain that is generally dependent on the level of strain, and hence do not have a unique or constant Young's modulus. Connective tissues such as the sclera and lamina cribrosa generally get stiffer as they are stretched.

Strain – It is a measure of the local deformation in a material or tissue induced by an applied stress, and is usually expressed as the percentage change in length of the original geometry (e.g., a wire that was originally 10 mm long that has been stretched an additional 1 mm, exhibits 10% strain). It is important to recognize that strain, unlike stress, may be observed and measured and it is strain, not stress, which causes damage to tissues.

Stress – It is a measure of the load applied to, transmitted through, or carried by a material or tissue, and can be defined as the amount of force applied to a tissue divided by the cross-sectional area over which it acts (e.g., pressure is a stress and can be expressed in pounds per square inch (psi)).

Structural stiffness – It is a composite measure of the entire structure's resistance to deformation that incorporates both the material properties and geometry of a complex load bearing system. In the posterior pole, both the geometry and material properties of the sclera and lamina cribrosa contribute to their structural stiffness, and hence determine the ability of the optic nerve head (ONH) and peripapillary sclera to withstand strain when exposed to intraocular pressure (IOP). As such, individual ONH biomechanics is governed by the geometry (size and shape of the scleral canal, scleral thickness, regional laminar density, and beam orientation) and the material properties (stiffness) of the lamina cribrosa and sclera. Hence, two eyes exposed to identical IOPs may exhibit very different strain fields due to differences in their structural stiffness.

Viscoelastic materials – These materials exhibit a stress–strain response that is time dependent, that is, they have higher resistance when loaded quickly than when loaded slowly (similar to the behavior of a hydraulic shock absorber).

*Adapted from Downs, C., Roberts, M. D., and Burgoyne, C. F. (2009). Mechanical strain and restructuring of the optic nerve head. In: Shaarawy, T. M., Sherwood, M. B., Hitchings, R. A., Crowston, J. G. (eds.) *Glaucoma Medical Diagnosis and Therapy*, vol. 1, pp 67–90. Philadelphia, PA: Saunders Elsevier.

The Optic Nerve Head as a Biomechanical Structure

The optic nerve head (ONH) is of particular interest from a biomechanical perspective because it is a weak spot within an otherwise strong corneo-scleral envelope. While there are likely to be important pathophysiologies within the lateral geniculate and visual cortex as well as evidence both for and against direct, intraocular pressure (IOP)-induced damage to the retinal photoreceptors, most evidence suggests that the lamina cribrosa is the principal site of retinal ganglion cell (RGC) axonal insult in glaucoma.

The lamina cribrosa provides structural and functional support to the RGC axons as they pass from the relatively high-pressure environment in the eye to a low-pressure region in the retrobulbar cerebrospinal space. To protect the RGCs in this unique anatomic region, the lamina cribrosa in higher primates has developed into a complex structure composed of a three-dimensional (3D) network of flexible beams of connective tissue (**Figure 1**). The ONH is nourished by the short posterior ciliary arteries, which penetrate the immediate peripapillary sclera to feed capillaries contained within the laminar beams. This intra-scleral and intra-laminar vasculature is unique in that it is encased in load-bearing connective tissue, either within the scleral wall adjacent to the lamina cribrosa, or within the laminar beams themselves (**Figure 1**). Glaucoma is a multifactorial disease, and we believe that biomechanics not only determines the mechanical environment in the ONH, but also mediates IOP-related reductions in blood flow and cellular responses through various pathways (**Figure 2**).

Consideration of the anatomy of the lamina cribrosa and peripapillary sclera suggests that the classic mechanical and vascular mechanisms of glaucomatous injury are inseparably intertwined (**Figures 1** and **2**). For example, prior to structural damage, purely IOP-related stress could detrimentally affect the blood supply to the laminar segments of the axons through deformation of the capillary-containing connective tissue structures. Also, IOP-related remodeling of the extracellular matrix (ECM) of the laminar beams could limit the diffusion of nutrients to RGC axons in the ONH. Reciprocally, primary insufficiency in the blood supply to the laminar region could

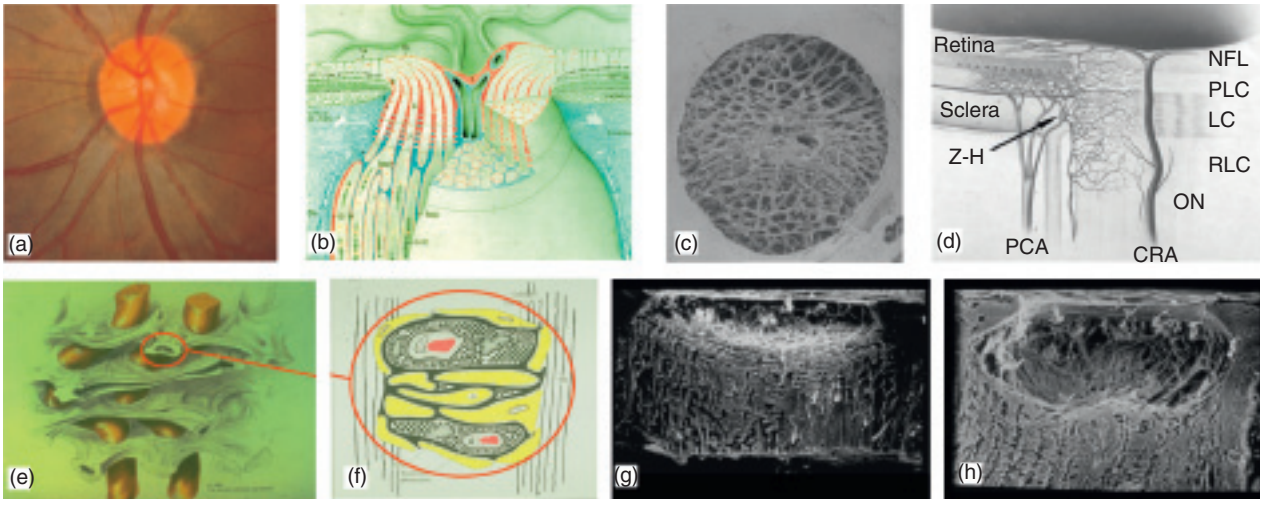

Figure 1 The optic nerve head (ONH) is a three-dimensional (3D) structure comprised of multiple interactive tissue systems that exist on different scales. This complexity has been a formidable deterrent to characterizing its mechanical environment. (a) While clinicians are familiar with the clinically visible surface of the optic nerve head (referred to as the optic disc), in fact the ONH (b) is a dynamic, 3D structure (seen here in an illustrated sectional view) in which the retinal ganglion cell (RGC) axons in bundles (white) surrounded by glial columns (red), pass through the connective tissue beams of the lamina cribrosa (light blue), isolated following trypsin digestion in an scanning electron micrograph (SEM) of the scleral canal in (c). The blood supply for the connective tissues of the lamina cribrosa (d) derives from the posterior ciliary arteries and the circle of Zinn-Haller (Z-H). (e, f) The relationship of the laminar beams to the axon bundles is shown in schematic form in (e). (f) Individual beams of the lamina cribrosa are lined by astrocytes. Together they provide structural and metabolic support for the adjacent axon bundles. Within the lamina, the RGC axons have no direct blood supply. Axonal nutrition requires diffusion of nutrients from the laminar capillaries (solid red), across the endothelial and pericyte basement membranes, through the extracellular matrix (ECM) of the laminar beam (stippled), across the basement membranes of the astrocytes (thick black), into the astrocytes (yellow), and across their processes (not shown) to the adjacent axons (vertical lines). Chronic age-related changes in the endothelial cell and astrocyte basement membranes, as well as intraocular pressure (IOP)-induced changes in the laminar ECM and astrocyte basement membranes may diminish nutrient diffusion to the axons in the presence of a stable level of laminar capillary volume flow. In advanced glaucoma, the connective tissues of the normal lamina cribrosa (sagittal view of the center of the ONH; vitreous above, orbital optic nerve below), (g) remodel and restructure into a cupped and excavated configuration (h). (b) Reprinted with permission from Doug Anderson; (c) reprinted with permission from Quigley HA; (d) reprinted with permission from Cioffi GA; (e) reprinted with permission from Quigley HA; (f) reprinted with permission from Morrison JC; (g, h) courtesy of Harry A. Quigley, MD.

induce cell-mediated connective tissue changes that would serve to weaken the laminar beams, making them more prone to failure under previously safe levels of IOP-related mechanical stress.

To incorporate these concepts into a global conceptual framework, we have previously proposed that the ONH is a biomechanical structure. This paradigm assumes that IOP-related stress (force/cross-sectional area) and strain (local deformation of the tissues) are central determinants of both the physiology and pathophysiology of the ONH tissues and their blood supply (**Figure 2**) at all levels of IOP. These stresses and strains are complex and can be separated into three components that act simultaneously: tension, compression, and shear (**Figure 3**). The distributions of stress, strain, and deformation are determined by the complex material properties and geometries of the sclera and lamina cribrosa (**Figures 4** and **5**). IOP-related stress and strain induce changes in the tissues that include not only alterations to the load-bearing connective tissues of the lamina cribrosa and the peripapillary sclera, but also the cellular components of these tissues, including astrocytes, glial cells, endothelial cells, and pericytes, along with their basement membranes and the RGC axons in the ONH. Experienced over a lifetime at physiologic levels, they underlie normal ONH aging. However, acute or chronic exposure to pathophysiologic levels results in glaucomatous damage.

Although clinical IOP-lowering remains the only proven method for preventing the onset and progression of glaucoma, the role of IOP in the development and progression of the disease remains controversial. This largely arises from the clinical observation that significant numbers of patients with normal IOPs develop glaucoma (e.g., normotensive glaucoma), while other individuals with elevated IOP show no signs of the disease. While there is a wide spectrum of individual susceptibility to IOP-related glaucomatous vision loss, the biomechanical effects of IOP on the tissues of the ONH likely play a

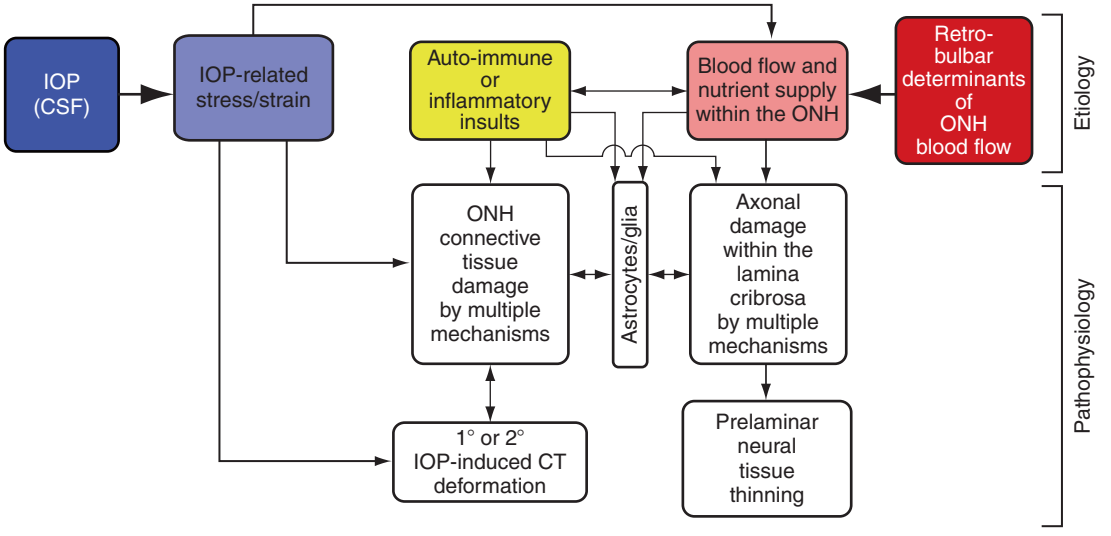

Figure 2 IOP-related stress and strain are a constant presence within the ONH at all levels of IOP. In a biomechanical paradigm, IOP-related strain influences the ONH connective tissues and the volume flow of blood (primarily), and the delivery of nutrients (secondarily) through chronic alterations in connective tissue stiffness and diffusion properties (explained in **Figure 1**). Non-IOP-related effects such as autoimmune or inflammatory insults (yellow) and retrobulbar determinants of ocular blood flow (red) can primarily damage the ONH connective tissues and/or axons, leaving them vulnerable to secondary damage by IOP-related mechanisms at normal or elevated levels of IOP. Based in part on Fig. 5, Burgoyne, C. F. and Downs, J. C. (2008). Premise and prediction – how optic nerve head biomechanics underlies the susceptibility and clinical behavior of the aged optic nerve head. *Journal of Glaucoma* 17(8): 318–328.

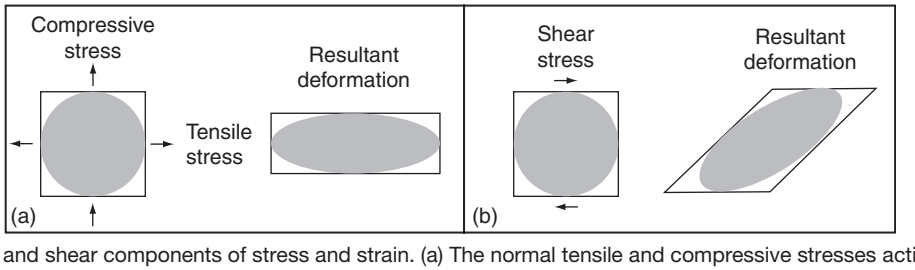

Figure 3 Normal and shear components of stress and strain. (a) The normal tensile and compressive stresses acting on a small square in the manner shown will act to elongate the region in one direction and compress it in the other. (b) The shear stresses acting on a similar region will act to distort the shape of the region.

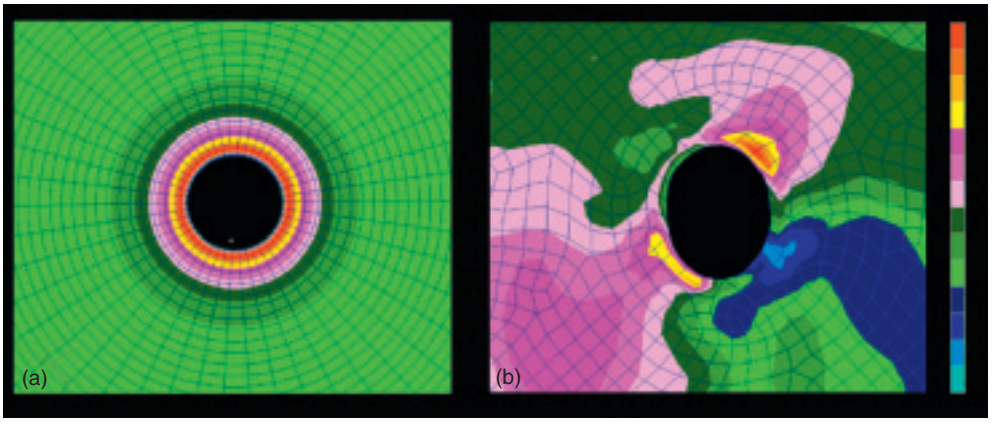

Figure 4 The material properties of the peripapillary sclera are influenced by nonlinearity and collagen fiber orientation (anisotropy). Separate from its thickness, the behavior of the sclera is governed by its material properties, which in turn are influenced by nonlinearity and fiber orientation. (a) Nonlinearity is an engineering term for tissues or structures whose material properties are altered by loading. Panel (a) demonstrates that the sclera becomes stiffer as it is loaded uniaxially (in one direction). In the case of the sclera, this is likely due to the fact collagen fibers embedded within the surrounding ground matrix start out crimped and progressively straighten as the load is increased. This conformational change in the fibrils accounts for the transition from an initially compliant, nonlinear response to a stiffened linear response as IOP increases. (b) Apart from nonlinearity, collagen fiber orientation (anisotropy) within the sclera strongly influences its mechanical behavior. Fiber orientation can be totally random (isotropic – not shown) or have a principal direction (anisotropic – three idealized cases shown). Finite element (FE) models of an idealized posterior pole with principal collagen fiber orientation in the circumferential, helicoidal, and longitudinal directions are shown. As the displacement plots show, the underlying fiber orientation can have profound effects on the deformation that occurs for a given IOP. Note that the displacement scale is exaggerated for illustrative purposes. Courtesy of Michael Girard.

central role in the development and progression of the disease at all IOPs. The individual susceptibility of a particular patient's ONH to IOP insult is likely a function of the biomechanical response of the constituent tissues and the resulting mechanical, ischemic, and cellular events driven by that response. Hence eyes with a particular combination of tissue geometry and stiffness may be susceptible to damage at normal IOP, while others may have a combination of ONH tissue geometry and stiffness that can withstand even high levels of IOP.

In this article, we focus on ocular biomechanics along two main themes: What is known about how mechanical forces and the resulting deformations are distributed in the posterior pole and ONH (biomechanics) and what is known about how the living system responds to those deformations (mechanobiology).

Mechanical Environment of the ONH and Peripapillary Sclera

Overview of the Mechanical Environment of the ONH and Peripapillary Sclera

From an engineering perspective, the eye is a vessel with inflow and outflow facilities that regulate its internal pressure. IOP imposes a pressure load normal to the inner surface of the eye wall, generating an in-wall circumferential stress known as the hoop stress (**Figure 6**). This IOP-generated stress is primarily borne by the stiff, collagenous sclera, while the more compliant retina and nerve fiber tissues bear little of the in-wall stress load and are therefore exposed primarily to the compressive stress of IOP. IOP is borne in the ONH by the fenestrated connective tissues of the lamina cribrosa, which span the scleral canal opening and tether into the stiff outer ring of circumferential collagen and elastin fibers in the peripapillary sclera (like a trampoline). While Laplace's law is useful to describe the pressure–deformation relationship in a spherical vessel of uniform thickness, it is inadequate for describing the eye's response to variations in IOP (**Figure 7**). There are several characteristics of the ocular load-bearing tissues that complicate the study of the mechanical environment to which the ONH and its resident cell populations are exposed.

First, the 3D connective tissue geometry of the eye is complex and difficult to measure. For instance, the thickness of monkey sclera can vary as much as fourfold from the equator to the peripapillary region and the 3D morphology of lamina cribrosa is more regionally complex and individualized than is generally appreciated. Second, the cornea, sclera and lamina cribrosa have extremely complex ECM microstructures with highly anisotropic collagen and elastin fibril orientations. As a result, the experimental characterization and theoretical/mathematical description of their constituent material properties are complex and difficult to obtain. Third, the cells that maintain the ocular connective tissues are biologically active. As such, the geometry and material properties of the sclera and lamina cribrosa change in response to both physiologic (age) and pathologic (IOP-related damage)

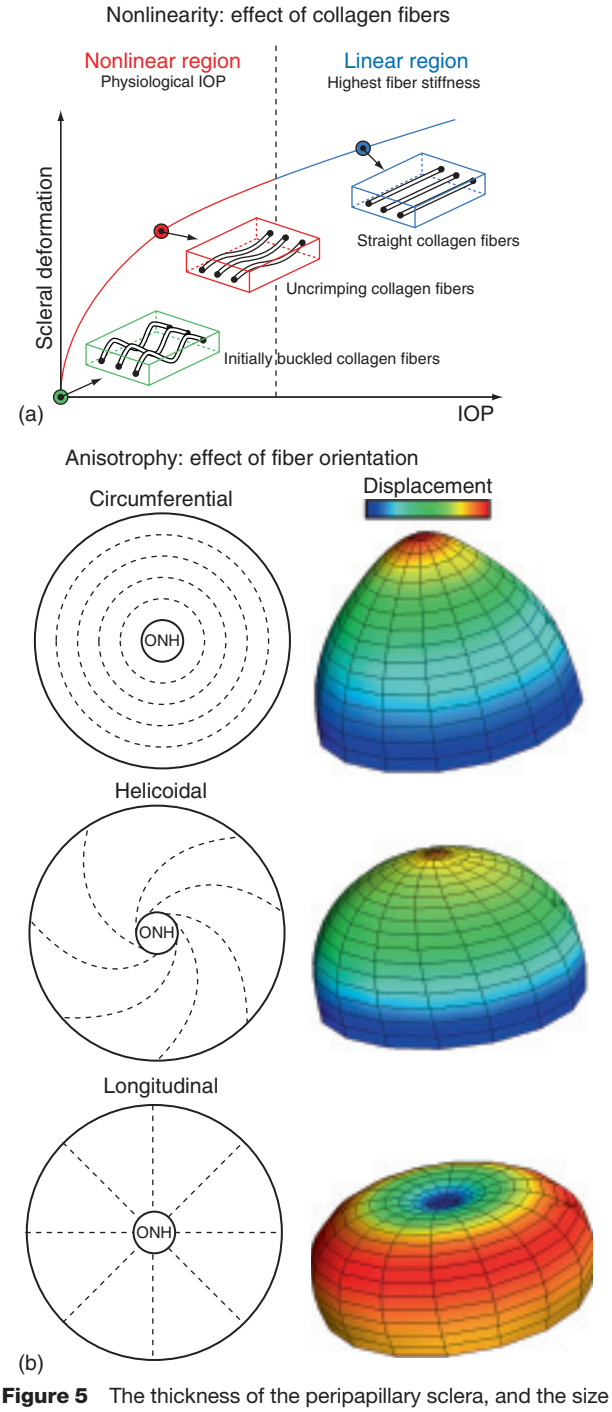

Figure 5 The thickness of the peripapillary sclera, and the size and shape of the scleral canal influence the magnitude and distribution of IOP-related stress within the peripapillary sclera. Stress plots within 3D biomechanical models of the posterior sclera and ONH demonstrate that stress concentrates around a defect (scleral canal) in a pressure vessel (eye) and varies according to the geometry of the peripapillary sclera and scleral canal. The idealized model in (a) shows the stress concentration around a circular canal in a perfectly spherical pressure vessel with uniform wall thickness (the ONH has been removed from these images for visualization purposes). The model in (b) shows the IOP-related stress concentration around an anatomically shaped scleral canal with realistic variation in peripapillary scleral thickness. In this case, the highest stresses (red) occur where the sclera is thinnest and the lowest stresses (blue) occur where the sclera is thickest, and also tend to concentrate around areas of the scleral canal with the smallest radius of curvature. The response of the sclera to this load is determined by its structural stiffness, which is the combination of geometry (how much tissue is bearing the load) and material properties (how rigid or compliant is the tissue).

factors. Fourth, the eye is exposed to ever changing loading conditions because IOP undergoes acute, short-term and long-term fluctuations ranging from blinks and eye rubs to circadian rhythms.

Finally, IOP-related stress generates strain patterns in the ONH and peripapillary sclera that are not only dependent on differing connective tissue geometries and material properties but are also influenced by complex loading conditions. The important factors contributing to this biomechanical component include the alignment and density of collagen fibrils in each tissue (stiffness and anisotropy), the rate of change in IOP (via tissue viscoelasticity), and the level of IOP-related strain at the time of altered loading (via tissue nonlinearity). In broad terms, the ONH connective tissues should be stiffer when there is already considerable strain present and/or if the IOP load is applied quickly. Conversely, the ONH should be more compliant in response to slow changes in IOP and/or at low levels of strain.

Mechanical Response of the ONH to Acutely Elevated IOP

It is important to note that the ONH responds to IOP elevations as a structural system, so the acute mechanical response of the lamina cribrosa is confounded with the responses of the peripapillary sclera, prelaminar neural tissues, and retrolaminar optic nerve. Also, because the lamina lies buried underneath the prelaminar neural tissues and the structural responses of these two tissue types to acute IOP elevations are quite different, acute laminar deformation cannot be directly measured or inferred by imaging the surface topography of the ONH. A final confounding effect is the cerebrospinal fluid pressure, which, along with IOP, determines the translaminar pressure gradient that must be borne by the lamina cribrosa.

Intuitively, it may seem that for a given acute increase in IOP, the lamina cribrosa should deform posteriorly and there have been several experimental studies designed to measure acute IOP-related laminar deformation. Yan and co-workers found that increasing IOP from 5 to 50 mmHg for 24 h produced an average posterior deformation of the central lamina of 79 μm in human donor eyes. Levy and Crapps reported a 12 μm average posterior movement of the central lamina with acute IOP elevations from 10 to 25 mmHg for shorter time periods in human eyes.

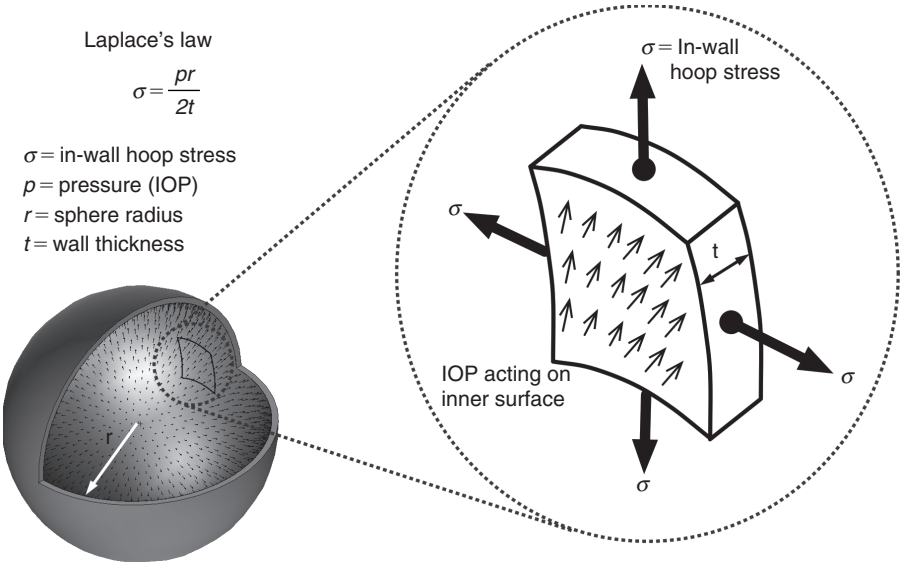

Figure 6 In-wall stress engendered by IOP loading. In an idealized spherical shell, the majority of the stress generated by IOP is transferred into a hoop stress borne within the thickness of the wall. Laplace's law, which relates the in-wall hoop stress to the internal pressure, is only applicable to spherical pressure vessels with isotropic material properties and uniform wall thickness, and can only be used to calculate very rough estimates of hoop stress in actual eyes. In pressure vessel geometries like the eye, with variable wall thickness, aspherical shape, and anisotropic material properties, the hoop stress may vary substantially by location.

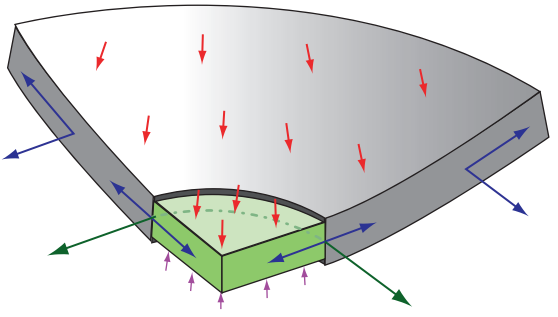

Figure 7 Stress, relative to IOP (red arrows) in the lamina cribrosa (light green) and peripapillary sclera (grey) engendered by IOP loading. Cut-away diagram of IOP-induced stress in an idealized spherical scleral shell with a circular scleral canal spanned by a more compliant lamina cribrosa. In this case, the majority of the stress generated by IOP (red arrows) is transferred into a hoop stress borne within the thickness of the sclera and lamina (blue arrows) that is concentrated circumferentially around the scleral canal (green arrows). Note that the difference between IOP (red arrows) and the retrolaminar cerebrospinal fluid pressure (pink arrows) is the translaminar pressure gradient that generates both a net posterior force on the surface of the lamina and a hydrostatic pressure gradient within the neural and connective tissues of the pre-laminar and laminar regions. Most importantly, note that the in-plane hoop stress transferred to the lamina from the sclera is much larger than stress induced by the translaminar pressure gradient.

More recently, Bellezza and colleagues reported a small but significant posterior laminar deformation of 10–23 µm (95% confidence interval (CI)) in a histologic evaluation of monkey eyes perfusion fixed with one eye at 10 mmHg and the contralateral eye at 30 or 45 mmHg for 15 min prior to death. However, these deformations, while statistically significant, did not substantially exceed the 95% CI for intra-animal physiologic differences (1–17 µm) between normal eyes bilaterally immersion fixed at an IOP of 0 mmHg.

The previous studies were performed using 2D measurements of laminar compliance within actual histologic sections. Angled sectioning, section warping, and the lack of a stable measurement reference plane can influence the accuracy of this technique. To overcome these problems, Downs, Yang and co-workers developed a technique for 3D delineation and measurement of ONH structures within high-resolution, digital 3D reconstructions (**Figure 8**). While our initial reports have concentrated on monkeys with early experimental glaucoma in one eye, preliminary data from a larger group of bilaterally normal monkeys perfusion fixed with both eyes at an IOP of 10 mmHg ($n = 5$), one eye at 10 mmHg, the other at 30 mmHg ($n = 3$), and one eye at 10 mmHg, the other at an IOP of 45 mmHg ($n = 3$) suggest that while acute IOP elevation causes expansion of the scleral canal, in most monkey eyes there is no net posterior laminar deformation from the plane of the sclera. Thus, our current understanding of the aggregate response of the young adult monkey ONH to acute IOP elevation is that expansion of the scleral canal tightens the lamina within the plane of the sclera, making it more resistant to posterior deformation out of that plane (**Figure 9**). These data are preliminary and our interpretation may change with further study.

It is important to note that the lack of laminar deformation in these eyes does not mean that the lamina is not

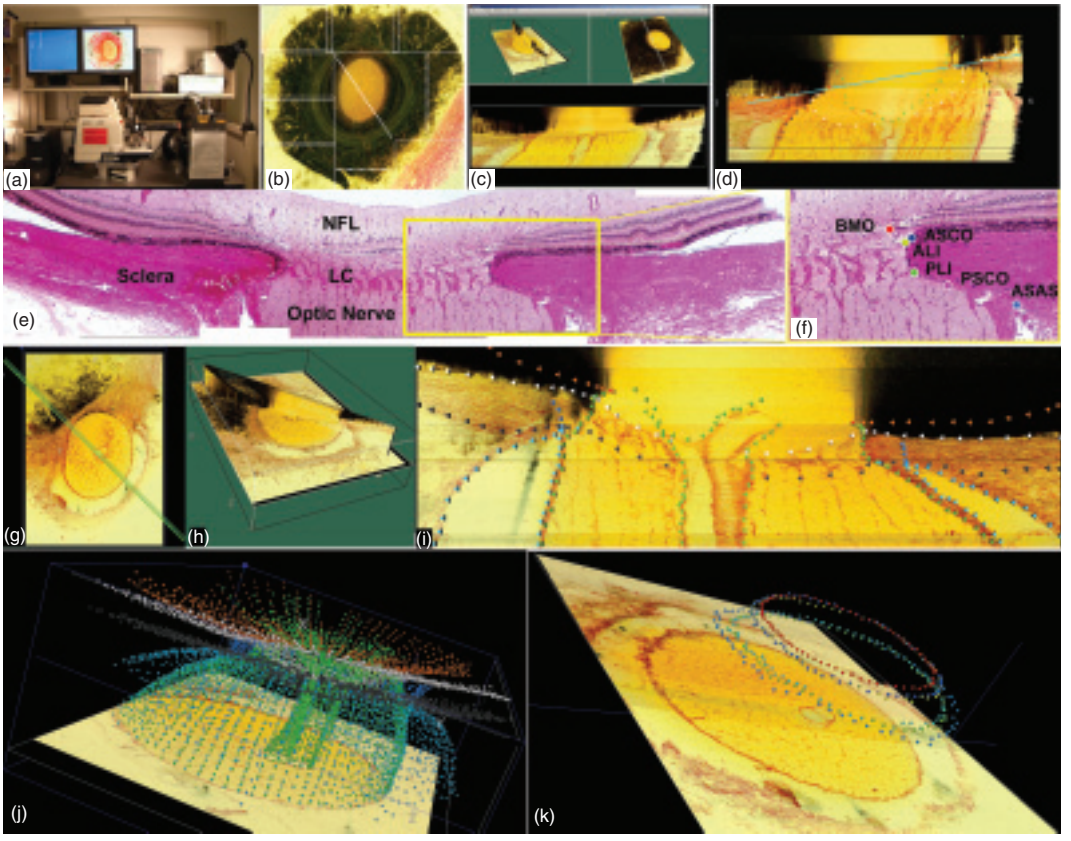

Figure 8 3D delineation of ONH and peripapillary scleral landmark points within digital 3D ONH reconstructions. (a) Photograph of our microtome-based 3D reconstruction device allows for serial sectioning and high-resolution image capture of the stained block face of embedded ONH specimens. (b) Images are acquired in a mosaic, then stitched into a composite of the entire 6-mm-diameter specimen, and stacked into a digital 3D reconstruction of the connective tissues of the ONH with 1.5 x 1.5 x 1.5 μm voxel resolution (c). Once loaded into custom software, the reconstruction can be digitally sectioned and landmarks delineated. In this view (d) our measurement reference plane, Bruch's membrane opening (BMO), is marked and shown with a light blue line. (e) Central horizontal histologic section through a representative normal monkey eye showing the ONH anatomy. (f) Magnified view of the nasal side of the neural canal showing the following landmark points: BMO (red), the anterior scleral canal opening (ASCO, dark blue), the anterior laminar insertion point (ALI, yellow), the posterior laminar insertion point (PLI, green), the posterior scleral canal opening (PSCO, pink), the anterior-most aspect of the subarachnoid space (ASAS, light blue). (g, h) With the 3D digital ONH reconstruction, a total of 40 radial, sagittal slices (each 7 voxels thick) are served to the delineator at 4.5° intervals. (i) A representative digital sagittal slice, showing the marks for seven landmark surfaces and six landmark point pairs. These features are interactively delineated within the 3D volume by viewing the position of a marking cursor displayed simultaneously within the sagittal (g) and transverse section images (h). (j) Representative 3D point cloud showing all delineated points for a normal monkey ONH in relation to the last section image of the reconstruction. (k) A subset of the 3D point cloud showing the neural canal landmarks depicted in (f).

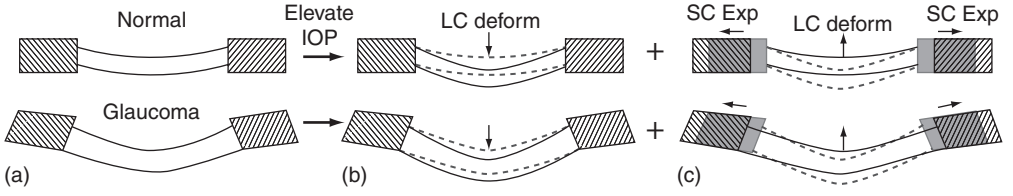

Figure 9 There are two components of acute IOP-induced ONH deformation in normal and early glaucoma eyes. (a) Sagittal section diagram of the ONH, showing the peripapillary sclera (hatched) and the lamina cribrosa for normal (upper) and early glaucoma (lower) eyes. Note that the early glaucoma eye has undergone permanent changes in ONH geometry including thickening of the lamina, posterior deformation of the lamina and peripapillary sclera, and posterior scleral canal expansion. Upon acute IOP elevation we believe two phenomena occur simultaneously and with interaction: the lamina displaces posteriorly due to the direct action of IOP (b), but much of this posterior laminar displacement is counteracted as the lamina is pulled taut by simultaneous scleral canal expansion (c). It is important to note that even though the net result of these IOP-related deformations is a small amount of posterior displacement of the lamina, substantial levels of IOP-related strain are induced in both the peripapillary sclera and lamina in this scenario.

strained. In this scenario, the expansion of the canal stretches the lamina cribrosa within the plane of the sclera generating substantial strain within the laminar beams. Estimation of laminar beam strain within these same 3D reconstructions is one of the outputs of finite element (FE) modeling, an engineering technique that is discussed in the section entitled 'Other acute, IOP-related changes in the ONH'.

The Contribution of the Sclera to ONH Biomechanics

The data described above, as well as the closed form analyses and computational models described in the next section suggest that the sclera plays an important role in ONH biomechanics. The peripapillary sclera provides the boundary conditions for the ONH. By this we mean that the peripapillary sclera is the tissue through which load and deformation are transmitted to the ONH, and that the structural stiffness of the peripapillary sclera, therefore, influences how the lamina deforms (**Figure 9**). This can be understood from the discussion above in which a compliant sclera allows the scleral canal to expand following an acute IOP elevation, tightening the laminar beams within the canal and thereby increasing laminar resistance to posterior deformation. In contrast, a rigid sclera allows less expansion of the canal or none at all, forcing the structural stiffness of the lamina alone to bear the IOP-related stress. Hence, characterization of both components of scleral structural stiffness (geometry and material properties) is essential to understanding the effects of IOP on the ONH.

Characterization of scleral geometry

Maps of the thickness variation for the posterior pole of human and monkey eyes show extreme spatial variation in scleral thickness, with very thin regions near the equator (as low as 300 μm in the human and 111 μm in the monkey). In both species the peripapillary sclera is notably thicker (1000 μm in the human and 415 μm in the monkey). Interestingly, this thick ring of peripapillary sclera is absent in the nasal quadrant of monkey eyes due to the oblique nasal insertion of the optic nerve through the scleral canal. Such variation in peripapillary scleral thickness as occurring naturally or in pathologic conditions such as myopia, may be important in assessing individual susceptibility to glaucomatous damage.

Characterization of scleral material properties

Several researchers have characterized scleral material properties in various species. Most recently, Downs and co-workers used a strain-rate controlled, servo-hydraulic materials testing system to determine the viscoelastic material properties of normal rabbit and monkey peripapillary sclera. They found that the material properties of peripapillary sclera are highly time dependent (viscoelastic), but reported no significant differences in material properties by quadrant.

However, uniaxial testing of scleral strips is limited in its ability to describe the nonlinear and anisotropic responses of the sclera (**Figure 5**), leading Girard and colleagues to develop a new 3D approach. Using a customized scleral shell pressurization apparatus, precise IOP control, and laser-based electronic speckle pattern interferometry, they measure the 3D deformation of the entire posterior scleral shell in response to small, stepped increases in IOP (from 5 to 45 mmHg). Results suggest that the monkey posterior sclera is highly nonlinear (it gets stiffer as IOP increases) and anisotropic (the underlying collagen fibril distribution is nonuniform and changes throughout the scleral shell, which affects directional stiffness) (**Figure 10**). By using an FE model backfitting method (see the following section), they have calculated the nonlinear, hyperelastic, anisotropic material properties for the entire posterior scleral shell of normal monkeys, and characterized changes in these properties due to age and stage of glaucomatous damage.

Engineering Models of Stress and Strain in the ONH and Peripapillary Sclera

Closed form solutions

Attempts to mathematically model the mechanical environment of the ONH generally fall into two broad categories – closed form solutions and numerical solutions. In closed form solutions, engineering principles are used to derive equations that can be analyzed to understand the effects of selected biological parameters. Examples of closed form approaches include work by Donqui, Edwards, and Good, and a hybrid cellular solid approach by Sander. The appeal of closed form solutions is that general conclusions may be drawn from a model cast in terms of a limited number of geometric and material parameters that are felt to be of interest or might be clinically measurable. However, closed form solutions may be of limited utility because of the complexity of the ONH and peripapillary scleral tissues (e.g., the nonuniform and asymmetric geometry and material properties). The most sophisticated of these studies suggest that the structural stiffness of the sclera is the most important determinant of macro-level ONH biomechanics.

Numerical solutions – FE analysis

To overcome the inherent limitations of closed form solutions, researchers often utilize numerical methods to study more complex biological systems. One of the most powerful of these is FE analysis. In FE analysis, complex load-bearing structures are broken into small, regularly shaped elements (**Figure 4**). Stress and strain within each element is calculated and then superposed to predict the mechanical response of the entire structure.

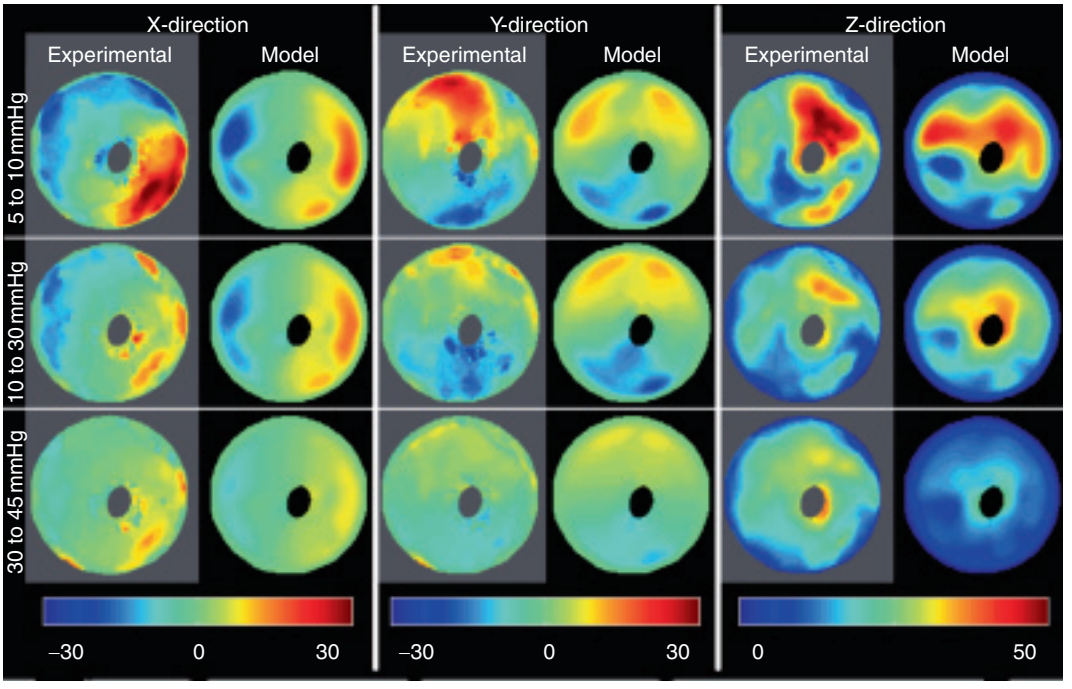

Figure 10 Experimental results and finite element (FE) model predictions of the nonlinear, anisotropic displacement behavior of an individual monkey posterior scleral shell as IOP increases from 5 to 10 mmHg (top row), 10 to 30 mmHg (middle row), and 30 to 45 mmHg (bottom row). Experimental (gray background) and predicted (model, black background) displacements for the X-direction (left-to-right), Y-direction (top-to-bottom), and Z-direction (in-and-out) are mapped onto the outer surface of the scleral shell of a right eye (for each map superior top, inferior bottom, temporal left and nasal right). The inhomogeneity of the experimental displacement patterns are indicative of underlying tissue anisotropy, and the much greater displacements seen in the 5–10 mmHg IOP elevation as compared to the 30–45 mmHg IOP elevation reflect the highly nonlinear behavior (i.e., the sclera is stiffer and therefore more resistant to deformation at higher levels of strain). Figure, including experimental and modeling results, courtesy of Michael Girard.

The power of FE analysis lies in its ability to model structures with highly complex geometries using material properties with varying levels of complexity as warranted (e.g., inhomogeneous, anisotropic, nonlinear, or viscoelastic material descriptions). The three components necessary as input for FE models are: the 3D geometry of the tissue structure to be modeled, the material properties of the different tissues in the model, and appropriate loading and boundary conditions. These requirements have spurred the development of methodologies to isolate and describe the 3D geometry of the ONH and peripapillary sclera (**Figure 8**) and experimentally characterize their constituent material properties (**Figure 10**).

There are two basic approaches to FE modeling of the ONH: parametric and individual specific. Parametric modeling involves computing stress and strain in average, idealized geometries that do not conform to any individual's particular anatomy. Within these models, parameters such as peripapillary scleral thickness and laminar stiffness can be varied independently to gauge the parameter's effects on ONH biomechanics as a whole. This is a similar approach to analytical modeling, but the analyzed geometries are much more fidelic and the results more relevant and intuitive. Although parametric FE models are by nature simplified in their geometries and there are limited cases that can be modeled, these investigations yield interesting insight into the contributions of individual anatomical elements and tissue material properties to overall ONH biomechanics.

Bellezza and colleagues used parametric FE modeling to study the mechanical environment of an idealized 3D model of the posterior pole. In this study, the effects of the size and shape (aspect ratio) of an elliptical scleral canal within a spherical scleral shell of uniform thickness were studied. Idealized beamlike structures spanning the ONH were also incorporated into the model to simulate the lamina cribrosa. This study illustrated that IOP-related stress concentrations within the load-bearing connective tissues of the ONH is substantial, even at low levels of IOP. Specifically, models with larger scleral canal diameters, more elliptical canals, and thinner sclera all showed increased stresses in the ONH and peripapillary sclera for a given level of IOP. In the peripapillary sclera and ONH, stresses were as much as one and two orders of magnitude greater than IOP, respectively. While the model used in this study was idealized in terms of its material properties and geometry, it served to reinforce the concept of the peripapillary sclera and ONH as a high stress environment even at normal levels of IOP.

Sigal and co-workers used idealized axisymmetric FE models to pursue a more complex parametric analysis of the factors that influence the biomechanical environment within the ONH (**Figure 11**). In these studies, various geometric and material details of a generic model were parametrized and independently varied to assess their impact on a host of outcome measures such as strain in the lamina cribrosa and prelaminar neural tissue (**Figure 11**). This work identified the five most important determinants of ONH biomechanics (in rank order) as: the stiffness of the sclera, the size of the eye, IOP, the stiffness of the lamina cribrosa, and the thickness of the sclera. The finding that scleral stiffness plays a key role in ONH biomechanics is especially interesting, and was also found to be important in the analytical models of Sander and co-workers. Parametric studies such as these are important because they can be used to identify important biomechanical factors that warrant more in-depth study, thus narrowing and focusing future experimental and modeling efforts.

To address the limitations of idealized geometric and material property descriptions inherent in parametric FE models, individual-specific FE models can be created from the reconstructed geometries of particular eyes. At present, individual-specific modeling is based on high-resolution 3D reconstructions of monkey and human cadaver eyes (**Figure 8**), with a long-term goal to build models based on clinical imaging of living eyes so as to use them in the assignment of target IOP. This is especially important given that the 3D geometry of the scleral canal and peripapillary sclera largely determines the stress and strain transmitted to the contained ONH (**Figure 7** notes specifically how the 3D geometry of the scleral canal and peripapillary sclera alter the stress environment). Anatomically accurate 3D models are necessary to capture the biomechanics of anisotropic scleral material properties (varying collagen fibril orientation), and scleral canals that are noncircular and have varying optic nerve insertion angles (i.e., the optic nerve inserts from the nasal side resulting in a thinner peripapillary sclera in that quadrant). When modeling an ONH with anatomic fidelity, the tissue geometries can be constructed either by serial histologic methods or by 3D imaging, and material properties are generally determined through direct mechanical testing (**Figure 10**). Unfortunately, imaging of the lamina *in vivo* is not yet possible at the resolutions required for modeling, and no technology exists for experimental biomechanical testing of laminar beams. As a result, ONH FE models are typically constructed from eyes that are perfusion or immersion fixed at a selected IOP, and then undergo *ex vivo* 3D reconstruction of their connective tissues.

Bellezza and co-workers developed a histologic technique to 3D reconstruct the trabeculated structure of the lamina cribrosa from individual monkey eyes that have been perfusion fixed at varying levels of IOP (**Figure 8**). The resulting 3D data sets form the geometries of individual-specific FE models of the ONH at the macro- and micro-scale. Roberts, Downs, and co-workers have developed macro-scale continuum FE models of the posterior pole and ONH connective tissues from individual monkey eyes (**Figure 12**). In these models, the laminar microarchitecture is modeled using a continuum approach, with anisotropic material properties assigned to each FE in the ONH based on the connective tissue volume fraction and the predominant beam orientation of the contained laminar microarchitecture (**Figure 13**). Regional variations in connective tissue volume fraction and predominant

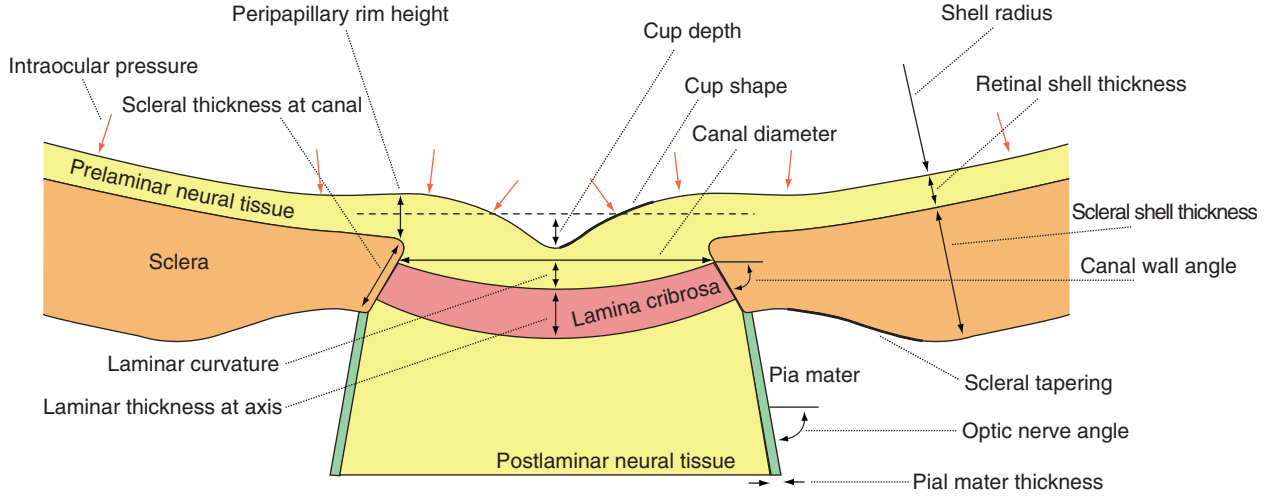

Figure 11 Parametric models can be used to study the influence of geometric and material property factors. To model the ONH, Sigal and colleagues created an idealized, axisymmetric (symmetric about the anterior-to-posterior axis) reference geometry and varied geometric and material property factors to assess their influence on various outcome measures of stress and strain within the model. This type of parametric sensitivity analysis is useful for identifying the tissues and anatomic structures that may be most important in the mechanical response of the ONH. Such information can serve to focus future biomechanics research and clinical device development efforts on the tissues and structures determined to be most important in ONH biomechanics. Figure courtesy of Ian Sigal.

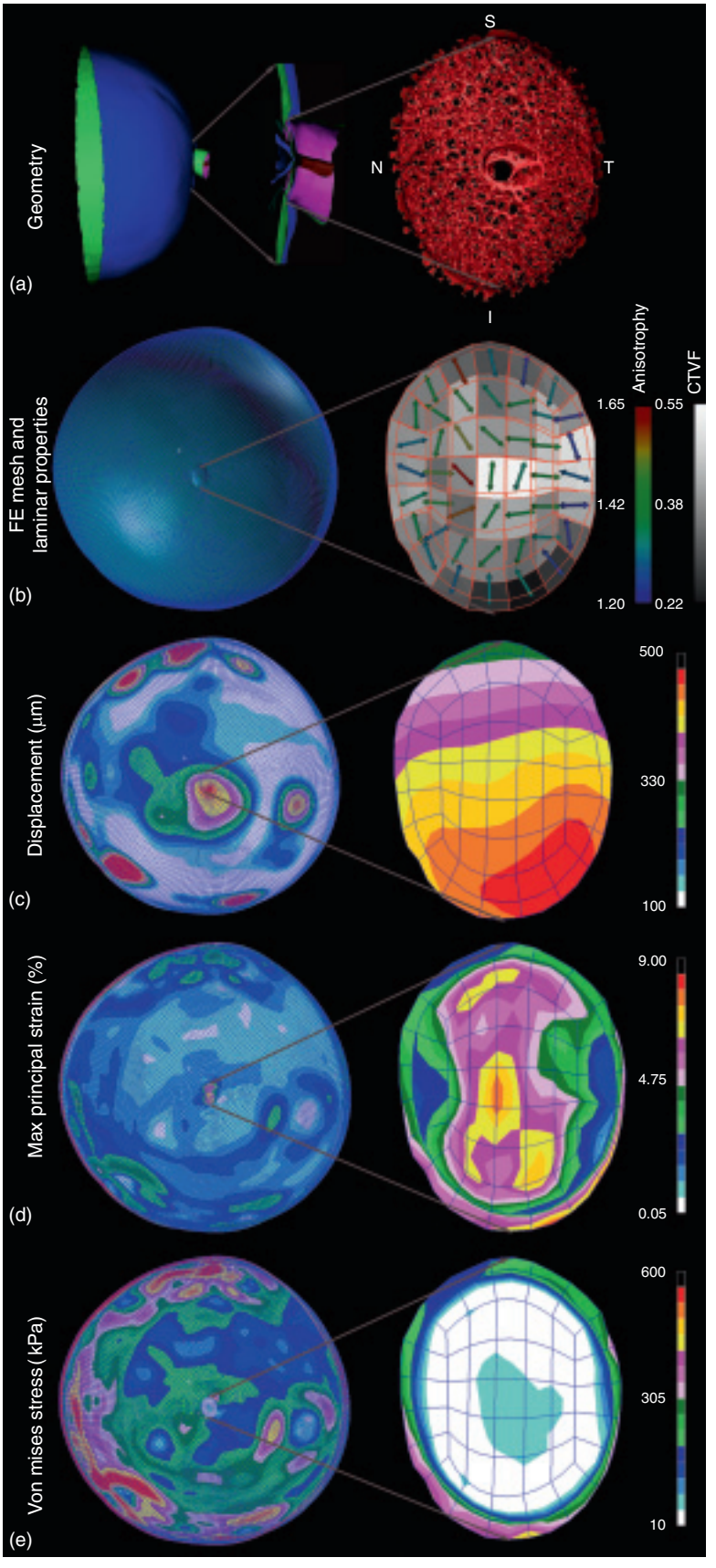

Figure 12 Construction and results from a macro-scale continuum FE model of the posterior scleral shell and ONH of a normal monkey eye. (a) To construct the model geometry, the 3D-delineated lamina cribrosa and surrounding peripapillary sclera (see **Figure 8**) of an individual eye are incorporated into a generic anatomic scleral shell with regional thickness variations mapped from previous

orientation are translated into variations in local oriented stiffness so that regions of higher and lower porosity reflect greater and lesser compliance, respectively. The inclusion of regional laminar material properties (connective tissue volume fraction and beam orientation) into FE models has a pronounced effect on the ONH's response to IOP (**Figure 14**). This indicates that the regional variations in laminar geometry and structural stiffness must be represented in models to fully capture the biomechanical behavior of the ONH and suggests that the lamina is biologically optimized to withstand IOP-induced deformation.

Downs and colleagues have also used the 3D reconstruction and continuum modeling approaches to characterize and explore laminar beam biomechanics. This micro-scale modeling approach utilizes a substructuring technique based on parent macro-scale FE models to calculate the IOP-related stress and strain fields in laminar beams (**Figure 15**). This technique reveals a complexity of IOP-related strains and stresses within the lamina cribrosa microarchitecture that is not available through macro-scale FE modeling. There have been several interesting preliminary results from this work. First, stress and strain in the laminar microarchitecture are likely higher than predicted by macro-scale models of the ONH. Second, even at normal levels of IOP, the micro-FE models predict that while the majority of laminar beams are within physiologic strain ranges, there are individual laminar beams with levels of IOP-related strain that are likely pathologic. Third, mean strain within the laminar beams of different

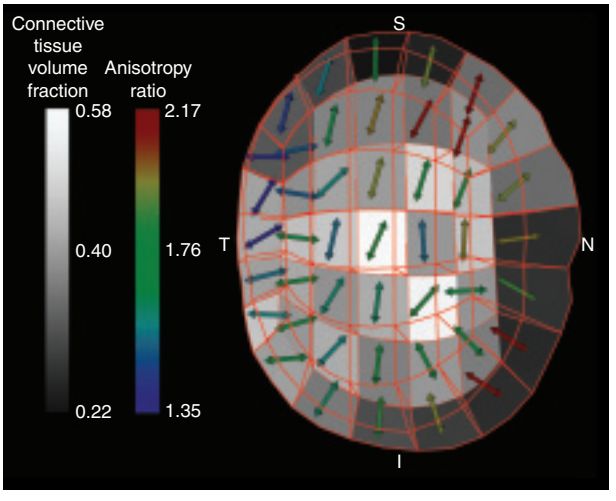

Figure 13 Regional differences in laminar microarchitecture in a normal monkey eye. Characterization of the laminar microarchitecture utilizes the element boundaries of a continuum finite mesh to partition the lamina cribrosa connective tissue into 45 subregions. The connective tissue volume fraction (CTVF) for each region is expressed as a percentage and mapped to a grayscale value in the background. The arrows indicate the predominant orientation of the laminar beams in each region, with higher values (color-coded) indicating regions in which the beams are more highly oriented. Note that in the peripheral regions of the lamina, the beams are tethered radially into the scleral canal wall.

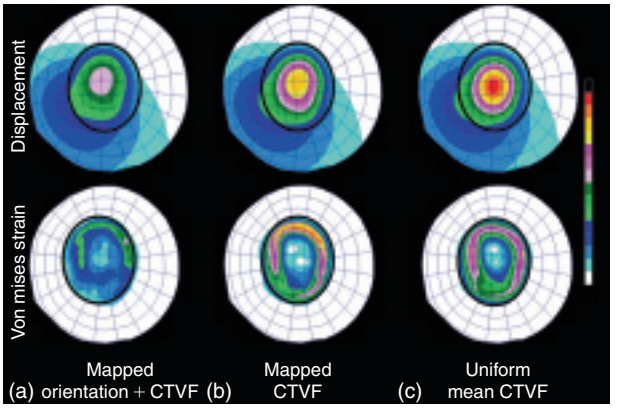

Figure 14 Incorporation of laminar beam orientation and connective tissue volume fraction into the material description of the lamina cribrosa affects the predictions of finite element (FE) models. Internal (vitreous) surface views of the displacement and strain in the ONH (within the heavy black outline) and peripapillary sclera in continuum models of the same eye following acute IOP elevation. In column (a), the stiffness of each laminar element is determined from both the predominant laminar beam orientation and connective tissue volume fraction (CTVF) of the contained lamina. In column (b) the orientation information (i.e., using an isotropic material stiffness), but retaining mapped CTVF produces a substantial increase in the displacement of the lamina with markedly higher strains. In column (c) all elements in the lamina are assigned the same isotropic material stiffness based on an average CTVF (with no beam orientation information). This model has slightly more central laminar displacement than case (b), but actually has lower strain in the superior lamina cribrosa owing to the fact that the superior elements in case (b) had lower CTVFs in that region (i.e., below the mean CTVF). These results suggest that representing regional laminar microarchitecture in FE models is essential to accurately predict ONH biomechanical behavior.

histologic measurements. The segmented 3D reconstruction of the laminar connective tissue (shown) is represented in each model. (b) A continuum FE mesh of the posterior pole is generated from the geometry. The sclera in this model is assigned uniform isotropic material properties based on previous experimental testing. The continuum elements representing the porous load-bearing laminar architecture are assigned anisotropic material properties that reflect the microstructure of the lamina enclosed by each laminar FE. This material property description is defined using a combination of the connective tissue volume fraction (CTVF) and the predominant laminar beam orientation. A visualization of the CTVF and predominant beam orientation are presented. Note that in this visualization, an anisotropy value of 1 would represent an isotropic material with no predominant orientation while larger values imply oriented laminar beams that impart higher stiffness in the direction of the plotted arrow. (c, d, e) FE results showing predicted displacement, strain, and stress distributions due to an increase in IOP from 10 to 45 mmHg. Note that in this eye, the model predicts that the ONH tilts inferiorly, the strains are highest along the superior–inferior axis of the ONH, and that the sclera bears most of the IOP-related stress.

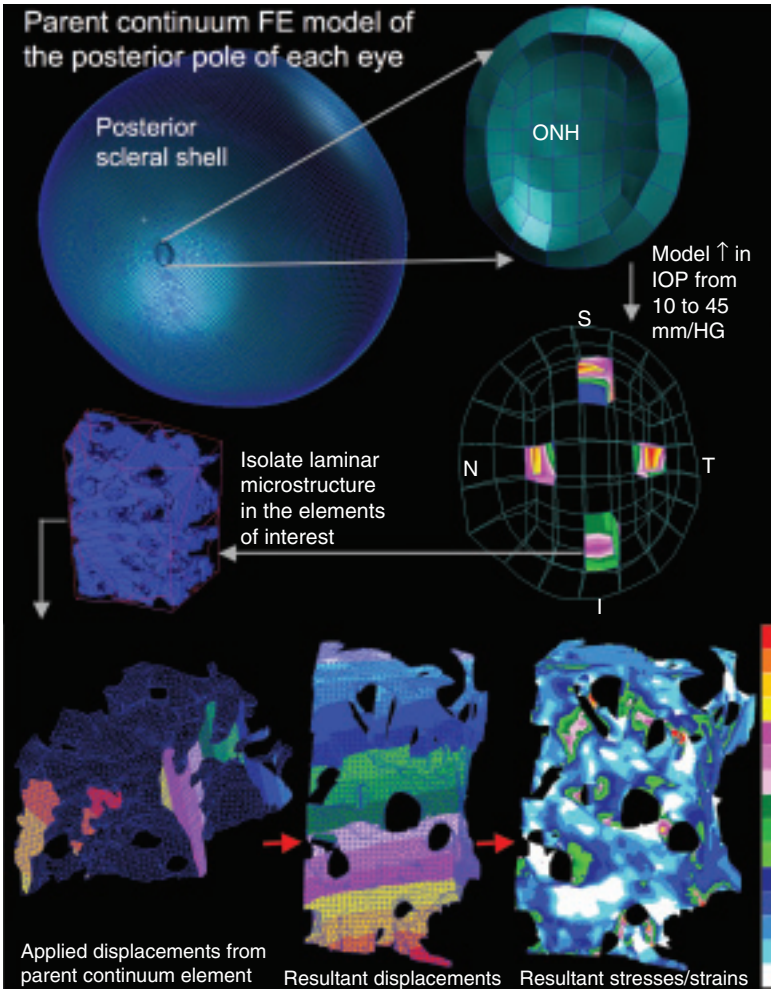

Figure 15 Construction and analysis of micro-FE models of the laminar microarchitecture of a monkey eye. The complexity of the stresses and strains at the laminar beam level is not captured in the macro-scale continuum FE models because the details of the microstructure are homogenized into a bulk material description. To address this limitation, a substructuring technique has been developed to characterize the beam-level strain environment within ONH models. The displacement field calculated from a continuum model is used along with individual element boundaries to define input loading conditions for micro-scale FE models of subregions of the 3D reconstructed lamina cribrosa. These micro-FE models illustrate that the stress and strain borne by the individual laminar beams are highly variable and complex. Modeling of individual beam mechanics will be necessary to predict the yield and failure of individual beams, model changes in blood flow in the laminar capillaries, and determine the strains to which laminar astrocyte basement membrane are subjected.

monkeys varies greatly, and is generally dependent on the 3D geometry of each eye's ONH connective tissues. Finally, strain is not equally distributed though the ONH, and are concentrated in regions with less dense laminar beams. This work, while still in its early stages, holds the possibility of testing hypotheses about failure mechanisms and cellular responses at the level of the laminar beams.

Other Acute, IOP-Related Changes in the ONH

ONH, retinal, and choroidal blood flow are all affected in different ways by acute IOP elevations. Previous studies using microspheres have suggested that volume flow within the prelaminar and anterior laminar capillary beds is preferentially diminished once ocular perfusion pressure (defined as the systolic arterial blood pressure plus one-third of the difference between systolic and diastolic pressures minus IOP) is less than 30 mmHg.

While a direct link to mechanical strain has not been established, axonal transport is compromised in the lamina cribrosa at physiologic levels of IOP and is further impaired following acute IOP elevations. Several hypotheses regarding this behavior emerge when considering ONH biomechanics. First, as the pores in the lamina cribrosa change conformation due to IOP-related mechanical strain, the path of the axons through those pores may be disrupted, thereby directly impeding axoplasmic

transport. Second, it may be that the IOP-related reduction in blood flow in the laminar region impairs the mitochondrial metabolism that drives axoplasmic transport. Finally, axoplasmic transport could be sensitive to the magnitude of the translaminar pressure gradient, and as that hydrostatic pressure gradient gets larger with increasing IOP (or lower cerebrospinal fluid pressure), the mechanisms driving that transport are unable to overcome the resistance of the pressure gradient (**Figure 7**).

In summary, while connective tissue dynamics should, by themselves, directly and indirectly influence astrocyte and glial metabolism and axonal transport, glaucomatous damage within the ONH may not necessarily occur at locations with the highest levels of IOP-related connective tissue strain, but rather at those locations where the translaminar tissue pressure gradient is greatest and/or where the axons, blood supply, and astrocytes and glia have been made most vulnerable. Further studies are necessary to elucidate the link(s) between IOP, mechanical strain, blood flow, astrocyte and glial cell homeostasis, and axoplasmic transport in the ONH, in both the physiologic and diseased states.

Restructuring and Remodeling of the ONH

Normal Aging

The ONH connective tissues are exposed to substantial levels of IOP-related stress and strain at normal levels of IOP (**Figure7**). We believe that physiologic levels of stress and strain experienced over a lifetime induce a broad spectrum of changes in both the connective tissues and vasculature that are central to normal aging. Thus, the restructuring and remodeling of glaucomatous damage (described in the following sections) should be understood to occur in the setting of the physiologic restructuring and remodeling inherent in normal aging.

Age-related alterations of the laminar ECM have been reported to include increased collagen deposition, thickening of astrocyte basement membranes, and increased rigidity of the lamina and sclera. Girard and colleagues have recently shown that the sclera in old monkeys is approximately twice as stiff than sclera from young monkeys at all IOPs. The aged ONH is thus more likely to have stiff connective tissues. Age-related hardening of the laminar ECM not only stiffens the connective tissues, it should also diminish nutrient diffusion from the laminar capillaries through the laminar ECM, across the astrocyte basement membranes, and into the adjacent axons (**Figure 1**). Thus, in addition to the effects of age-related decreases in the volume flow within the laminar capillaries, axonal nutrition in the aged eye may be further impaired as a result of diminished nutrient diffusion from the laminar capillaries to the center of the axon bundles.

Alterations in Connective Tissue Architecture, Cellular Activity, Axoplasmic Transport, and Blood Flow in Early Glaucoma

Pathophysiologic stress and strain induce pathologic changes in cell synthesis and tissue microarchitecture that exceed the effects of aging and underlie the two governing pathophysiologies in glaucoma: (1) mechanical yield and/or failure of the load-bearing connective tissues of the ONH (**Figures 2** and **16**) and (2) progressive damage to the adjacent axons by a variety of mechanisms (**Figure 2**).

Early glaucomatous damage has not been rigorously studied in humans because human cadaver eyes with well-characterized early damage are rare. In monkeys, following moderate experimental IOP elevations, we have described the following changes in ONH and peripapillary scleral connective tissue architecture and material properties at the onset of confocal scanning laser tomography-detected ONH surface change (clinical cupping): (1) enlargement and elongation of the neural canal (**Figure 17**); (2) posterior deformation and thickening of the lamina cribrosa accompanied by mild posterior deformation of the scleral flange and peripapillary sclera (**Figure 18**); (3) hypercompliance of the lamina in some cases; and (4) alteration in the viscoelastic material properties of the peripapillary sclera. These findings are accompanied by prelaminar neural tissue thickening and are summarized in **Figure 19**.

Roberts and coworkers have shown that in the monkey model of early experimental glaucoma, the volume of the laminar connective tissues is approximately 80% larger in the glaucoma eyes compared to their contralateral controls. The most surprising result of that work is the nature of that addition of laminar volume. Their results suggest that the connective tissues in glaucomatous eyes remodel in a way that the immediate retrolaminar septa add connective tissue and are recruited into the 3D load-bearing structure of the lamina.

The increase in laminar thickness in these early glaucoma monkey eyes is likely a combination of axonal swelling, tissue edema, gliosis, connective tissue remodeling, and new connective tissue synthesis. Preliminary quantification of the amount of connective tissue within our 3D reconstructions of the lamina suggests an increase in connective tissue volume of 50–100% in early glaucoma (**Figure 20**). These data strongly support the notion that connective tissue remodeling, and new connective tissue synthesis, are present at this early stage of the neuropathy.

Alterations in cellular activity, axoplasmic transport and blood flow in early glaucoma have not been rigorously studied. However, in a recent study in rat eyes (which has a very minimal lamina cribrosa), Johnson and colleagues used genomic techniques to characterize the alterations in the genome of ONH tissues following 5 weeks exposure to experimental elevated IOP. Within

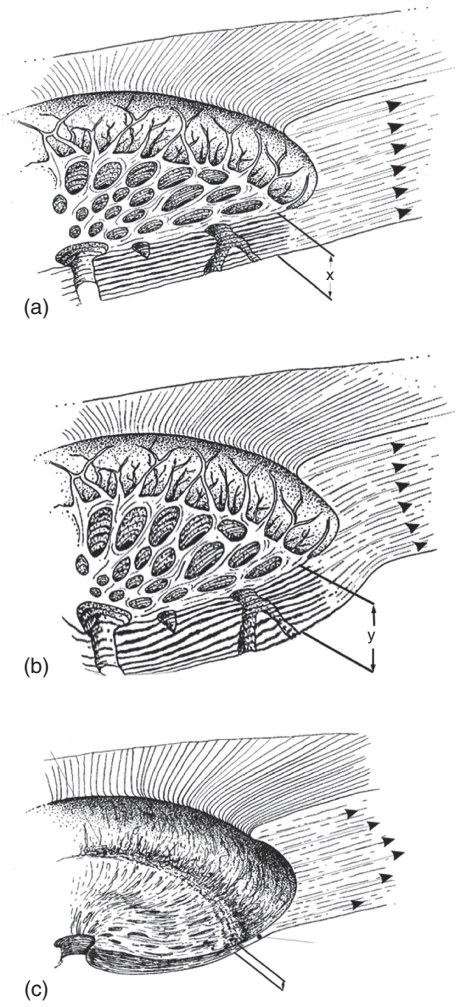

Figure 16 Progression of connective tissue morphology from normal health to early glaucoma to end-stage glaucoma. (a) Diagram of normal ONH connective tissue showing the thickness of the lamina cribrosa (x) and the in-wall hoop stress generated by IOP in the peripapillary sclera. (b) In early experimental glaucoma, our data to date suggests that rather than catastrophic failure of the laminar beams, there is permanent posterior deformation and thickening (y) of the lamina which occurs in the setting of permanent expansion of the posterior scleral canal. These changes indicate that a combination of mechanical yield and subsequent remodeling of the connective tissues occur very early in glaucoma that is not yet accompanied by physical disruption of the beams or frank excavation. (c) As the disease progresses to end-stage damage, we believe that the anterior laminar beams eventually fail, the lamina compresses (z) and scars, the laminar insertion into the sclera displaces posteriorly, and the scleral canal enlarges to the typical cupped and excavated morphology. Very little is known about the biomechanics, cellular processes, and remodeling that drives the morphological progression from the earliest detectable stage of glaucoma to end-stage damage, but it is likely that these processes continue to be driven by the distribution of IOP-related stress and strain within the connective tissues either primarily or through their effects on the capillaries contained within the laminar beams and the adjacent astrocytes. Modified from Burgoyne, C. F. and Downs, J. C. (2008). Premise and prediction – how optic nerve head biomechanics underlies the susceptibility and clinical behavior of the aged optic nerve head. *Journal of Glaucoma* 17(8): 318–328.

the large group of animals studied, a subset of eyes had an early focal stage of orbital optic nerve axon loss. Within these animals, expression of genes governing initiation of cell division was maximally elevated (compared to later stages of damage) as well as the genes for several ECM components including fibulin 2, tenascin C, and the matrix metalloproteinase inhibitor TIMP-1. While gene expression for transforming growth factor (TGFβ1) increased linearly with severity of damage in all studied eyes, gene expression for TGFβ2 was lowest in the focally damaged eyes suggesting differential expression of TGFβ isoforms at this early stage of the neuropathy. Similar to TGFβ2, gene expression for the principal water channel protein in astrocytes, aquaporin-4, demonstrated the largest degree of downregulation in focal damage. Most importantly, Johnson and co-workers characterized gene expression patterns in a group of 2-week optic nerve transection eyes and found a pattern of expression similar to the most severely damaged high IOP eyes, suggesting that the changes in gene expression in the focal group were likely IOP-related, not simply a reflection of early axonal loss.

Alterations in Connective Tissue Architecture, Cellular Activity, Axoplasmic Transport, and Blood Flow in Later Stages of Glaucomatous Damage

The classic descriptions of profound laminar deformation, excavation of the scleral canal beneath the optic disk margin, compression, and increased rigidity of the lamina are largely based upon human and monkey eyes with moderate, severe, and end-stage glaucomatous damage. Because these studies describe a broad range of damage that has occurred in response to an IOP insult that is uncharacterized in magnitude and duration, a common description of events has yet to emerge. However, astrocyte basement membrane disruption and thickening as well as damage to elastin, physical disruption of the laminar beams, and remodeling of the ECM are consistent phenomenon within these reports. It is assumed that IOP-induced alterations in the synthetic activities of the cells associated with these tissues underlie these changes.

Within the more severely damaged eyes in Johnson's study (above), expression of genes governing initiation of cell division was also elevated (compared to normals) but to a lesser degree than in eyes with focal damage. Genes associated with activation of microglia, immune response, ribosomes, and lysosomes were all linearly elevated in the more severely damaged eyes. Genes for the ECM components including fibulin 2, tenascin C, and the matrix metalloproteinase inhibitor TIMP-1 were elevated nonlinearly (most elevated in early damage, elevated less in more severe), whereas genes for periostin, collagen IV,

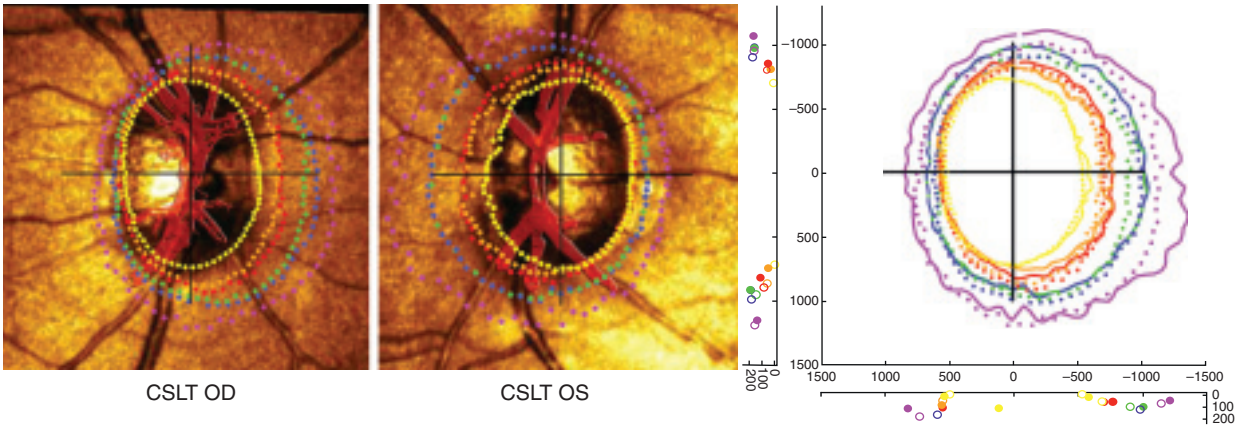

Figure 17 (left and middle) Our method of 3D reconstruction and delineation (**Figure 8**) includes the central retinal vessels, which allows clinical alignment of the delineated point clouds to clinical images and demonstrates the anatomic expansion of the neural canal under the clinically visible disc margin. Here just the Neural Canal landmark points are three-dimensionally overlaid onto Heidelberg Retinal Tomograph images of the normal (OD, left) and early experimental glaucoma (OS, middle) eye of a monkey. Note that the clinically visible disk margin in these eyes has been histomorphometrically determined to be BMO (yellow dots) in both eyes. Note also that the neural canal is not the size of the clinical visible disk margin, but rather it enlarges dramatically as it passes through the sclera. Because the data are digital, the left eye data can be converted to right eye orientation and overlaid onto the right eye data as shown in (right). Here the early glaucoma (solid line) and normal (dotted line) eye data can be directly compared. Note that expansion of the neural canal is present at the onset of early glaucomatous damage in the monkey eye and is greatest in the posterior aspects of the canal.

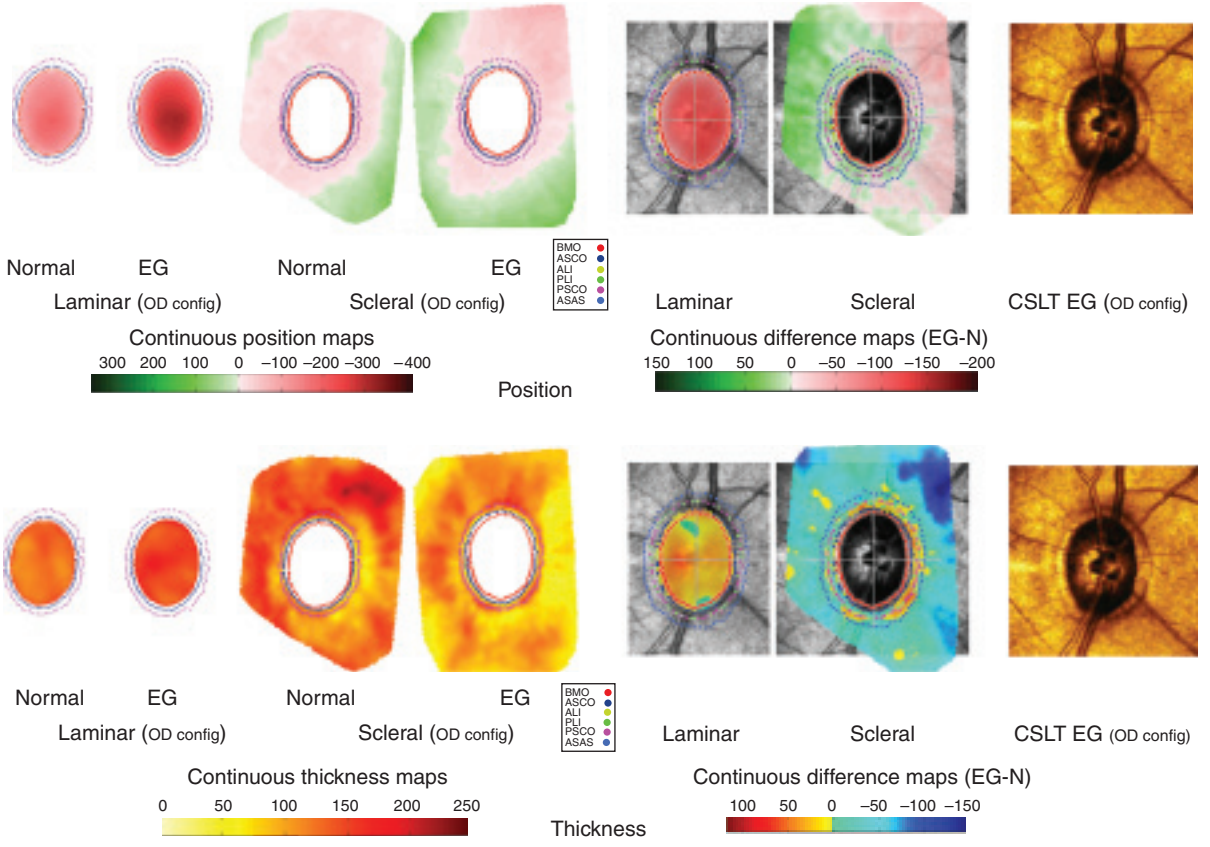

Figure 18 3D histomorphometric maps of laminar and peripapillary scleral position and thickness demonstrate profound permanent posterior deformation of the lamina cribrosa and peripapillary sclera and thickening of the lamina cribrosa in the early glaucoma eye of one monkey. Laminar and peripapillary scleral position (above) and thickness (below) are co-localized with the neural canal landmark points for both the normal and early glaucoma eyes of one monkey (left four columns). Early glaucoma eye difference maps for each parameter are shown in the first two columns to the right, followed by a Confocal Scanning Laser Tomograph image of the early glaucoma eye prior to sacrifice for orientation. These maps are typical for early glaucomatous changes in the monkey eye and demonstrate the permanent posterior deformation of the lamina and immediate peripapillary sclera, as well as the marked thickening of the lamina in the glaucoma eye compared to its contralateral control.

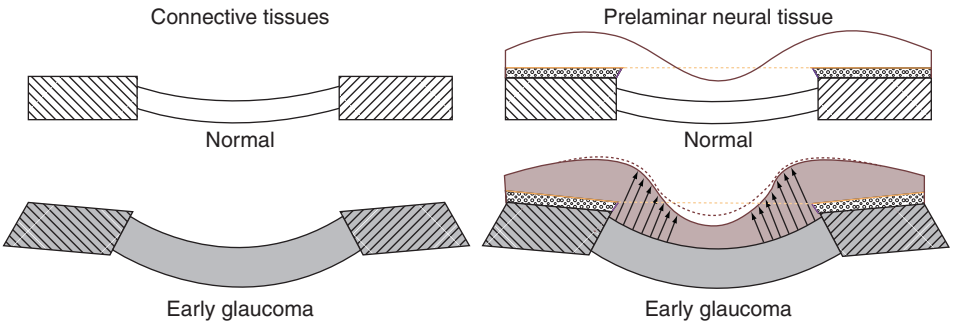

Figure 19 Remodeling and restructuring of the ONH in early experimental glaucoma. Sagittal section diagrams of the ONH, showing the peripapillary sclera (hatched) and the lamina cribrosa for normal and early glaucoma eyes. (left) The early glaucoma eye has undergone permanent changes in ONH geometry, including thickening of the lamina, posterior deformation of the lamina and peripapillary sclera, and posterior scleral canal expansion. (Right) Recent work has also shown that although the cup deepens relative to Bruch's membrane opening (dotted orange line) as can be detected by longitudinal confocal scanning laser tomography imaging (orange line) in early glaucoma, the prelaminar neural tissues (gray) are actually thickened rather than thinned. Reprinted with permission from Hongli Yang.

and collagen VI were elevated linearly. Differential gene expression for TGFβ1 and TGFβ2, as well as nonlinear expression of aquaporin are described above.

Axoplasmic transport alterations at the lamina cribrosa and a complicated array of ONH, retinal and choroidal blood flow alterations have been described following chronic IOP elevation in monkey and human eyes. However, direct observation of ONH blood flow at the level of the peripapillary sclera and lamina cribrosa capillaries is not yet possible either experimentally or clinically. We thus lack the ability to study primary interactions between IOP and non-IOP-induced alterations in ONH blood flow, ONH connective tissue integrity, ONH glial cell activity, and RGC axonal transport within individual human and animal eyes.

Integrins are mechanotransduction proteins that span the laminar astrocyte and capillary endothelial cell basement membranes to bind to ligands in the ECM and interact with the cell cytoskeleton. Morrison has described the location and alteration of integrin subunits in normal and glaucomatous human and monkey eyes and proposed them as an important link between laminar deformation and damage, laminar connective tissue remodeling, and laminar astrocyte mediated axonal insult in glaucoma.

Biomechanical Manipulation of ONH and Peripapillary Scleral Cells in Culture

Laminar astrocytes have been shown to respond to changes in hydrostatic or barometric pressure. However, the uncertain role of hypoxia and lack of astrocyte basement membrane deformation in the barometric pressure model has led to genomic and biochemical characterization of ONH astrocytes exposed to controlled levels of strain. At present, these strain-based techniques are in their infancy and a consistent stimulation cycle and pattern of gene and protein expression has yet to emerge. Eventually, strain predictions from FE models and data on IOP fluctuation from telemetric IOP monitoring studies will allow these experiments to more closely model physiologic/pathophysiologic conditions in the normal and glaucomatous human and animal eye.

Future Directions

Clinical Implications

There are currently no science-based tools to predict at what level of IOP an individual ONH will be damaged. As described herein, FE modeling is a computational tool for predicting how a biological tissue of complicated geometry and material properties will behave under varying levels of load. The goal of basic research FE modeling in monkey and human cadaver eyes is to learn what aspects of ONH neural, vascular, and connective tissue architecture are most important to the ability of a given ONH to maintain structural integrity, nutritional and oxygen supply, and axoplasmic transport at physiologic and nonphysiologic levels of IOP. In the future, clinical imaging of the ONH will seek to capture the architecture of these structures so as to allow clinically derived biomechanical models of individual patient ONHs to make predictions regarding physiologic and pathophysiologic levels of IOP. Eventually knowing the relationship between IOP, mechanical strain, systemic blood pressure, and the resultant astrocyte and axonal mitochondrial oxygen levels will drive the clinical assessment of safe target IOP. Clinical characterization of the actual IOP insult through telemetric IOP monitoring will eventually allow better-controlled studies of ONH directed neuroprotection. Finally, these FE modeling-driven targets for deep (subsurface) ONH imaging will likely allow early detection of lamina cribrosa deformation and thickening. Once clinically

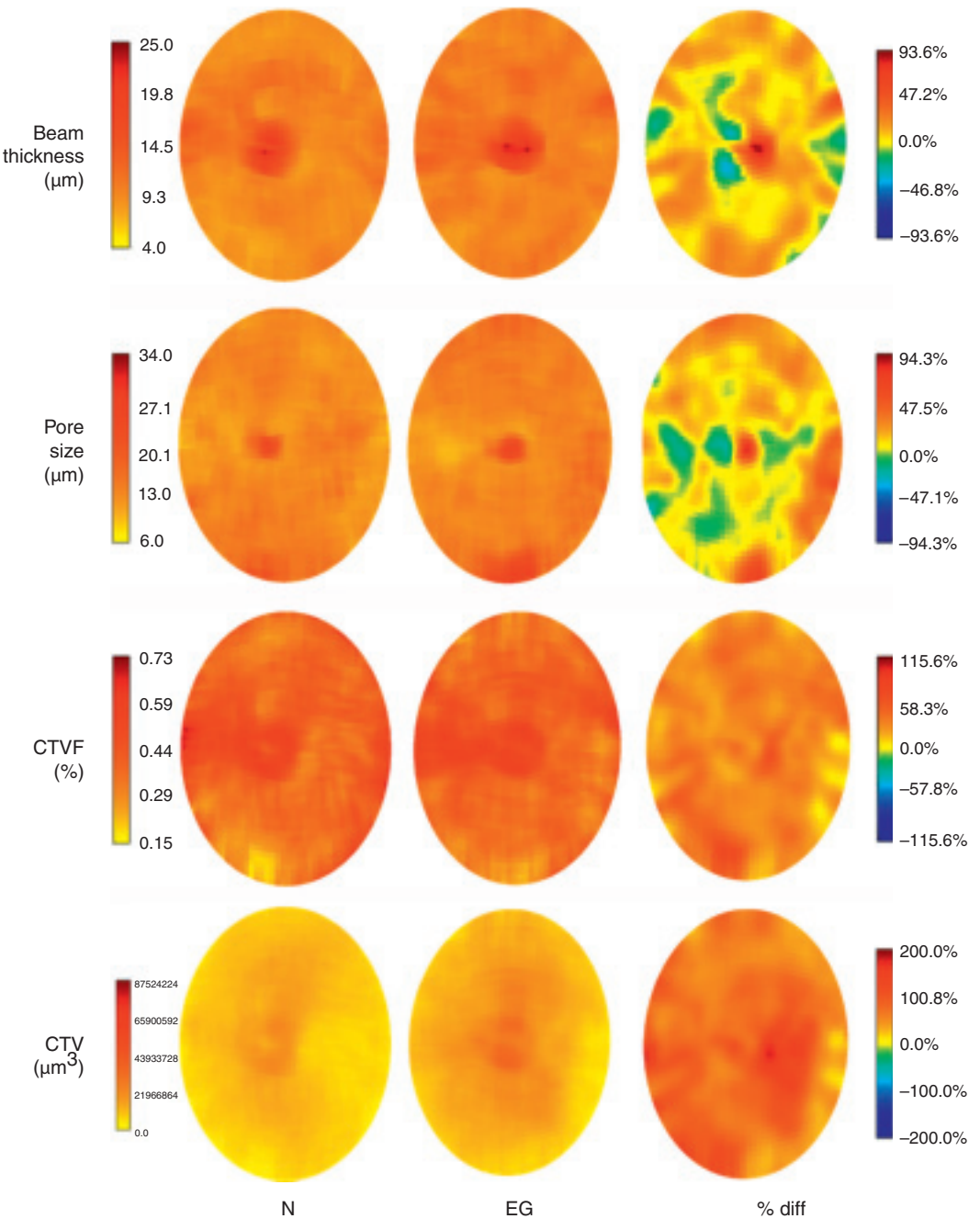

Figure 20 3D histomorphometric maps of laminar microarchitecture in paired and normal and early glaucoma eyes for three monkeys (left and center). Maps of laminar beam thickness, pore size, connective tissue volume fraction (CTVF), and connective tissue volume (CTV) for contralateral normal and early glaucoma eyes of a monkey derived from the same 3D reconstruction technique described in **Figure 8**. (Right) The differences between the normal and early glaucoma eyes for each parameter are mapped as a percentage. Note that CTVF is ratio of laminar connective tissue volume to total tissue volume in each regional sample. In early glaucoma, the CTVF and total laminar connective tissue volume increase significantly in all regions, and laminar beam thickness and pore size increase in most regions but decrease in others. These results together indicate that the increase in laminar thickness described in **Figure 18** in early experimental glaucoma, is due not just to axonal swelling or tissue edema, but also contains a very substantial component of laminar connective tissue synthesis.

detectable, early stabilization, and perhaps reversal, of these laminar changes will become a new end point for target IOP lowering in most ocular hypertensive and all progressing eyes.

Basic Research Directions

From an engineering standpoint, large challenges remain to achieve basic and clinical knowledge regarding: (1) the mechanisms and distributions of IOP-related yield and

failure in the laminar beams and peripapillary sclera; (2) the mechanobiology of the astrocytes, scleral fibroblasts, and lamina cribrosa, and glial cells; (3) the mechanobiology of axoplasmic flow and within the lamina cribrosa; (4) the fluid dynamics governing the volume flow of blood within the laminar capillaries and scleral and laminar branches of the posterior ciliary arteries; and (5) nutrient diffusion to the astrocytes in young and aged eyes. We predict that knowledge gained from these studies will importantly contribute to new therapeutic interventions aimed at the ONH and peripapillary sclera of glaucomatous eyes.

See also: Animal Models of Glaucoma; Intraocular Pressure and Damage of Optic Nerve Axons; Primary Open-Angle Glaucoma; Retinal Ganglion Cell Apoptosis and Neuroprotection.

Further Reading

Albon, J., Purslow, P. P., Karwatowski, W. S., and Easty, D. L. (2000). Age-related compliance of the lamina cribrosa in human eyes. *British Journal of Ophthalmology* 84: 318–323.

Burgoyne, C. F. and Downs, J. C. (2008). Premise and prediction – how optic nerve head biomechanics underlies the susceptibility and clinical behavior of the aged optic nerve head. *Journal of Glaucoma* 17(8): 318–328.

Burgoyne, C. F., Downs, J. C., Bellezza, A. J., Suh, J. K.-F., and Hart, R. T. (2005). The optic nerve head as a biomechanical structure: A new paradigm for understanding the role of IOP-related stress and strain in the pathophysiology of glaucomatous optic nerve head damage. *Progress in Retinal and Eye Research* 24: 39–73.

Clark, A. F., Browder, S. L., Steely, H. T., et al. (1995). Cell biology of the human lamina cribrosa. In: Drance, S. M. and Anderson, D. R. (eds.) *Optic Nerve in Glaucoma*, pp. 79–105. Amsterdam: Kugler Publications.

Downs, J. C., Roberts, M. D., and Burgoyne, C. F. (2008). The mechanical environment of the optic nerve head in glaucoma. *Optometry and Vision Science* 85(6): 425–435.

Geijer, C. and Bill, A. (1979). Effects of raised intraocular pressure on retinal, prelaminar, laminar, and retrolaminar optic nerve blood flow in monkeys. *Investigative Ophthalmology and Visual Science* 18: 1030–1042.

Girard, M. J. A., Suh, J.-K. F., Bottlang, M., Burgoyne, C. F., and Downs, J. C. (2009). Scleral biomechanics in the aging monkey eye. *Investigative Ophthalmology and Visual Science* 50. (doi:10.1167/iovs.08-3363).

Hernandez, M. R., Andrzejewska, W. M., and Neufeld, A. H. (1990). Changes in the extracellular matrix of the human optic nerve head in primary open-angle glaucoma. *American Journal of Ophthalmology* 109: 180–188.

Kirwan, R. P., Fenerty, C. H., Crean, J., et al. (2005). Influence of cyclical mechanical strain on extracellular matrix gene expression in human lamina cribrosa cells *in vitro*. *Molecular Vision* 11: 798–810.

Morrison, J. C. (2006). Integrins in the optic nerve head: potential roles in glaucomatous optic neuropathy (an American Ophthalmological Society thesis). *Transactions of the American Ophthalmological Society* 104: 453–477.

Quigley, H. and Anderson, D. R. (1976). The dynamics and location of axonal transport blockade by acute intraocular pressure elevation in primate optic nerve. *Investigative Ophthalmology and Visual Science* 15: 606–616.

Roberts, M. D., Grau, V., Grimm, J., et al. (2009). Remodeling of the connective tissue microarchitecture of the lamina cribrosa in early experimental glaucoma. *Investigative Ophthalmology and Visual Science* 50(2): 681–690.

Sigal, I. A., Flanagan, J. G., and Ethier, C. R. (2005). Factors influencing optic nerve head biomechanics. *Investigative Ophthalmology and Visual Science* 46: 4189–4199.

Sigal, I. A., Roberts, M. D., Girard, M., Burgoyne, C. F., and Downs, J. C. (2009). Biomechanical changes of the optic disk. In: Levin, L. A. and Albert, D. M. (eds.) *Ocular Disease: Mechanisms and Management,* 1st edn., ch. 20. London: Elsevier.

Yang, H., Downs, J. C., Girkin, C. A., et al. (2007). 3-D histomorphometry of the normal and early glaucomatous monkey optic nerve head: Lamina cribrosa and peripapillary scleral position and thickness. *Investigative Ophthalmology and Visual Science* 48: 4597–4607.